Journal of Quantitative Spectroscopy & Radiative Transfer 165 (2015) 88–92

Contents lists available at ScienceDirect

Journal of Quantitative Spectroscopy & Radiative Transfer

journal homepage: www.elsevier.com/locate/jqsrt

Fast far-field calculation in the discrete dipole approximation

Patrick C. Chaumet*, Ting Zhang, Anne Sentenac

Aix Marseille Université, CNRS, Centrale Marseille, Institut Fresnel UMR 7249, 13013 Marseille, France

ARTICLE INFO

Article history:
Received 12 March 2015
Received in revised form
22 June 2015
Accepted 29 June 2015
Available online 7 July 2015

Keywords:
Discrete dipole approximation
Electromagentic scattering
Far field computation
Computation of differential cross-section

ABSTRACT

The discrete dipole approximation is an efficient technique for simulating the field radiated by a particle of any shape. In this approach, the object is viewed as a collection of radiating electric dipoles. The field scattered by the particle is obtained by summing the fields radiated by each dipole. When the particle size is much larger than the wavelength, this technique is time consuming. We propose a Fourier based method which permits a significant reduction of the computation time.

© 2015 Elsevier Ltd. All rights reserved.

1. Introduction

Electromagnetic scattering by an arbitrary three-dimensional object can be simulated rigorously with different methods: finite difference in time domain method, finite element method, and volume integral method [1]. All these methods solve numerically the Maxwell equations without any approximation (except the numerical discretization and truncation). In this paper we focus on the volume integral method or more particularly on the discrete dipole approximation (DDA) [2–4]. This method has the advantage to be applicable to inhomogeneous, anisotropic objects.

The DDA can be described as a two step process. The first step, which is the main bottleneck of the approach, consists in finding the field inside the object by solving a self consistent equation discretized into a dense linear system. Intensive research, combining the use of symmetry properties, fast Fourier transforms (FFT) for the matrix vector products [5] and iterative solvers [6–9], has permitted to accelerate significantly this calculation. The DDA, once limited to objects of typical volume comparable to the incident wavelength cubed, can now tackle objects larger than a thousand wavelength cubed in a reasonable time (depending on their permittivity contrast) [9,10].

The second step consists in computing the scattered field at the required observation points. Recently Flatau and Draine have proposed a very efficient numerical scheme for calculating the field radiated close to the object [11] but, to our knowledge, no effort was brought on the far-field calculation.

Now, while a straightforward computation of the far-field takes very little time for small objects, it becomes time-consuming when the object size reaches hundreds of wavelength cubed and when many observation points are required. For large weakly contrasted objects it can even last longer than the calculation of the field inside the object. This situation is encountered for example in optical microscopy, in holography [12–14], or in flow cytometry [15] applications, which require to calculate the far-field of soft optical objects (generally biological samples) on a large grid of scattering angles. Thus, improving the DDA far-field computation is now necessary for extending the application domain of this approach. In this work, we propose a means to diminish drastically its computational cost by using Fast Fourier transforms.

2. Theory

In this section, we briefly sketch the DDA principles [16,17] and investigate the use of Fast Fourier transforms for accelerating the far-field computation.

* Corresponding author.
E-mail address: patrick.chaumet@fresnel.fr (P.C. Chaumet).

http://dx.doi.org/10.1016/j.jqsrt.2015.06.024
0022-4073/© 2015 Elsevier Ltd. All rights reserved.

2.1. Expression of the field inside the object with the DDA

The object, in free space, is described by its permittivity ε at the nodes of a regularly discretized box with dimension $L_x = N_x d_x$, $L_y = N_y d_y$ and $L_z = N_z d_z$ where d_x, d_y and d_z are the sizes of the discrete dipole along the different axis. Hereafter, for simplicity we will assume that the mesh is cubic with $d_x = d_y = d_z = d$ but the derivation applies also to cuboid mesh [18].

The object is illuminated by a monochromatic incident wave $\mathbf{E}_0$ with wavenumber $k_0 = \omega/c$ where ω is the frequency and c denotes the speed of light in vacuum. The local fields at subunit i_x, i_y, i_z is

$$\mathbf{E}(\mathbf{r}_{\{i\}}) = \mathbf{E}_0(\mathbf{r}_{\{i\}}) + \sum_{\{j\},\{i\}\neq\{j\}}^{\{N\}} \mathbf{T}(\mathbf{r}_{\{i\}},\mathbf{r}_{\{j\}})\mathbf{p}_{\{j\}}. \tag{1}$$

where $\{i\} = i_x, i_y, i_z$ and $\{N\} = N_x, N_y, N_z$. $\mathbf{T}$ denotes the dyadic field-susceptibility tensor of free-space, $\mathbf{p}$ is the dipole moment of each subunit of discretization, such

$$\mathbf{p}_{\{j\}} = 0 \quad \text{if } \mathbf{r}_{\{j\}} \notin \Omega \tag{2}$$

$$\mathbf{p}_{\{j\}} = \alpha(\mathbf{r}_{\{j\}})\mathbf{E}(\mathbf{r}_{\{j\}}) \quad \text{if } \mathbf{r}_{\{j\}} \in \Omega, \tag{3}$$

where $\alpha(\mathbf{r}_{\{j\}})$ is the polarizability of the subunit $\{j\}$ with the radiative reaction term [16] and Ω is the three dimensional region occupied by the scatterer. If we write Eq. (1) for all $N = N_x N_y N_z$ subunits forming the object, we get a linear system of size $3N \times 3N$ which is solved iteratively.

2.2. Expression of the scattered field under the DDA

Once the local field is known at each subunit position, the scattered field is classically computed for any observation point $\mathbf{r}$ outside the object as

$$\mathbf{E}_{\mathrm{d}}(\mathbf{r}) = \sum_{\{j\}=1}^{\{N\}} \mathbf{T}(\mathbf{r},\mathbf{r}_{\{j\}})\mathbf{p}_{\{j\}}. \tag{4}$$

If $\mathbf{r}$ is far from the object ($r \gg l^2/\lambda$ where l is the characteristic size of the object and λ the illumination wavelength), the dyadic field-susceptibility tensor can be replaced by its asymptotic form and the Eq. (4) reads

$$\mathbf{E}_{\mathrm{d}}(\mathbf{r}) = k_0^2 \frac{e^{ik_0 r}}{r} \sum_{\{j\}=1}^{\{N\}} e^{-i\mathbf{k}\cdot\mathbf{r}_{\{j\}}} \left[\mathbf{p}_{\{j\}} - \mathbf{n}\left(\mathbf{n}\cdot\mathbf{p}_{\{j\}}\right)\right] \tag{5}$$

where $\mathbf{n} = \mathbf{r}/r$ and $\mathbf{k} = k_0\mathbf{n}$.

The field at the image plane of an optical microscope requires the evaluation of $\mathbf{E}_{\mathrm{d}}$ for all the observation directions $\mathbf{k}$ allowed by the numerical aperture of the objective. The phase function of a particle necessitates to calculate the differential scattering cross-section (which is proportional to $|r\mathbf{E}_{\mathrm{d}}(\mathbf{r})|$) for all $\mathbf{k}$. In practice, a finite number N_o of directions $\mathbf{k}$ is taken with a sampling related to the object size (the bigger the object the finer the sampling rate). Now, if N and N_o are large, the computation time required by the sum in Eq. (5) which is proportional to $N \times N_o$ may become prohibitive. Thus it can be useful to perform this sum using the fast Fourier transform.

2.3. Computation of the scattered far-field using two-dimensional fast Fourier transforms

Eq. (5) can be rewritten as

$$\mathbf{E}_{\mathrm{d}}(\mathbf{r}) = k_0^2 \frac{e^{ik_0 r}}{r} \sum_{j_z=1}^{N_z} e^{-ik_z z_{j_z}} \times \left[\sum_{j_x=1 j_y=1}^{N_x,N_y} e^{-i(k_x x_{j_x} + k_y y_{j_y})}\mathbf{p}_{\{j\}} - \mathbf{n}\left(\mathbf{n}\cdot\sum_{j_x=1 j_y=1}^{N_x,N_y} e^{-i(k_x x_{j_x} + k_y y_{j_y})}\mathbf{p}_{\{j\}}\right)\right]. \tag{6}$$

In Eq. (6) the sum $\sum_{j_x=1 j_y=1}^{N_x,N_y} e^{-i(k_x x_{j_x} + k_y y_{j_y})}\mathbf{p}_{\{j\}}$ can be calculated with two-dimensional fast Fourier transform routine via,

$$\widehat{\mathbf{p}}(k_x,k_y) = \sum_{j_x=1 j_y=1}^{N_x,N_y} e^{-i(k_x x_{j_x} + k_y y_{j_y})}\mathbf{p}_{\{j\}} = \sum_{j_x=1 j_y=1}^{\widehat{N}_x,\widehat{N}_y} e^{-i(k_x x_{j_x} + k_y y_{j_y})}\overline{\mathbf{p}}_{\{j\}}, \tag{7}$$

where $(\widehat{N}_x, \widehat{N}_y)$ are the number of points used by the FFT along the x or y direction. Notice that $\overline{\mathbf{p}}_{\{j\}} = \mathbf{p}_{\{j\}}$ if $j_x \le N_x$ and $j_y \le N_y$ else $\overline{\mathbf{p}}_{\{j\}} = 0$. This implies that the step in the frequency domain along the x and y directions, $\Delta k_{x(y)}$ are equal to $2\pi/(d\widehat{N}_{x(y)})$. Hence $\widehat{\mathbf{p}}(k_x,k_y)$ is computed for $k_x = i_x\Delta k_x$ and $k_y = i_y\Delta k_y$ for $i_x = -\widehat{N}_x/2, \ldots, \widehat{N}_x/2-1$ and $i_y = -\widehat{N}_y/2, \ldots, \widehat{N}_y/2-1$, respectively.

Once $\widehat{\mathbf{p}}(k_x,k_y)$ is obtained it is easy to deduce $\mathbf{E}_{\mathrm{d}}$ in the direction k_x and k_y from Eq. (6) using $k_z = \sqrt{k_0^2 - k_x^2 - k_y^2}$.

2.4. Computation of the scattered far-field using three-dimensional fast Fourier transforms

Eq. (5) can be also written as

$$\mathbf{E}_{\mathrm{d}}(\mathbf{r}) = k_0^2 \frac{e^{ik_0 r}}{r}\left[\sum_{j_x=1 j_y=1 j_z=1}^{N_x,N_y,N_z} e^{-i(k_x x_{j_x} + k_y y_{j_y} + k_z z_{j_z})}\mathbf{p}_{\{j\}} - \mathbf{n}\left(\mathbf{n}\cdot\sum_{j_x=1 j_y=1 j_z=1}^{N_x,N_y,N_z} e^{-i(k_x x_{j_x} + k_y y_{j_y} + k_z z_{j_z})}\mathbf{p}_{\{j\}}\right)\right]. \tag{8}$$

One may use a three dimensional fast Fourier transform of $\mathbf{p}$ by casting Eq. (8) in the form:

$$\widehat{\mathbf{p}}(k_x,k_y,k_z) = \sum_{j_x=1 j_y=1 j_z=1}^{N_x,N_y,N_z} e^{-i(k_x x_{j_x} + k_y y_{j_y} + k_z z_{j_z})}\mathbf{p}_{\{j\}} \tag{9}$$

$$\widehat{\mathbf{p}}(k_x,k_y,k_z) = \sum_{j_x=1 j_y=1 j_z=1}^{\widehat{N}_x,\widehat{N}_y,\widehat{N}_z} e^{-i(k_x x_{j_x} + k_y y_{j_y} + k_z z_{j_z})}\overline{\mathbf{p}}_{\{j\}}. \tag{10}$$

This technique may be interesting if the object has similar dimensions in the x, y, z directions. On the other hand, it yields only an approximation of the far-field. Indeed, for a

given $k_x = j_x \Delta k_x, k_y = j_y \Delta k_y$ one cannot find $k_z = j_z \Delta k_z$ that is exactly equal to $\sqrt{k_0^2 - k_x^2 - k_y^2}$.

3. Results

The computation of the far-field using Fast Fourier transforms is particularly well-adapted to applications in microscopy or holography [12] as it yields the scattered far-field on a rectangular grid of transverse wavevectors (k_x, k_y) which is exactly what is obtained on the pixels of a camera. This sampling is also very efficient for estimating the scattering pattern of an object as it paves quite regularly the observation sphere.

In this section, we compare the accuracy and computation-time of the far-field calculation using the FFT approaches (Eqs. (6) and (8)) as compared to that of the classical estimation (Eq. (5)). To simplify the analysis, we do not provide here a study of the angular distribution of the scattered far-field but focus on useful integrated values, the total scattering cross-section and asymmetry factor which give a good idea of the global accuracy of the far-field calculation.

Several techniques have been developed to estimate these quantities with the DDA approach depending on the technique used for their estimation [10,19]. One of them consists in integrating the flux of scattered Poynting vector through a sphere enclosing the particle and thus requires to calculate the scattered far-field (Eq. (5)) along many directions. Generally the integration is performed in spherical coordinates (with constant polar and azimuthal angular spacing) [16] so that the total scattering cross section reads

$$C_{\rm sca} = \frac{k_0^4}{|E_0|^2} \int_0^{\pi} \int_0^{2\pi} \sin\theta \left| \sum_{\{j\}=1}^{\{N\}} \left[\mathbf{p}_{\{j\}} - \mathbf{n}\left(\mathbf{n}\cdot\mathbf{p}_{\{j\}}\right)\right] e^{-i\mathbf{k}\cdot\mathbf{r}_{\{j\}}} \right|^2 \mathrm{d}\theta\, \mathrm{d}\phi. \tag{11}$$

If fast Fourier transforms are used for calculating the far-field, Eqs. (6) and (8), an integration in Cartesian coordinates is more natural. In this case, the scattering cross-section reads

$$C_{\rm sca} = \frac{k_0^4}{|E_0|^2} \int_{S_1+S_2} \frac{1}{k_0 k_z} \left| \sum_{\{j\}=1}^{\{N\}} \left[\mathbf{p}_{\{j\}} - \mathbf{n}\left(\mathbf{n}\cdot\mathbf{p}_{\{j\}}\right)\right] e^{-i\mathbf{k}\cdot\mathbf{r}_{\{j\}}} \right|^2 \mathrm{d}k_x\, \mathrm{d}k_y, \tag{12}$$

where the integral $\int_{S_1+S_2}$ denotes a surface integration over two discs of radius k_0 with $k_z = \sqrt{k_0^2 - k_x^2 - k_y^2}$ for S_1 and $k_z = -\sqrt{k_0^2 - k_x^2 - k_y^2}$ for S_2.

In the following, we study the scattered cross-section $C_{\rm sca}$ and the asymmetry parameter g of spheres of refractive index 1.1 in air illuminated by a plane wave along the z axis estimated by the three different approaches. The accuracy of the results is estimated by forming the relative error with respect to Mie theory.

We first compare the accuracy of the integration in spherical coordinates, Eq. (11), to that of the integration in Cartesian coordinates (Eq. (12)) for calculating the scattering cross-section and the asymmetry parameter of a sphere of diameter 5λ. The same number of discretization points were taken for both integration schemes. We observe in Fig. 1 that the Cartesian discretization yields much better results than the spherical discretization. This was to be expected since the Cartesian coordinates samples the integration sphere more regularly than the spherical one.

Hereafter, all the integrals are performed in Cartesian coordinates, Eq. (12), with the same sampling rate Δk. Hence, the only difference between the different approaches stems from the estimation of the far-field which is performed either by the classical approach (Eq. (5)), the 2D FFT technique (Eq. (6)) or the 3D FFT (Eq. (8)). Note that, if the same mesh size d is taken for both the classical and 2D FFT approach, the far-field estimated along the same direction by Eq. (5) is identical to that given by Eq. (6) as we compute exactly the same integral. Thus, when the integrals are performed in Cartesian coordinates, the accuracy of the classical technique is the same as that of the 2D FFT approach.

We study in Fig. 2 the influence on the computation-time, Fig. 2(a), and accuracy, Fig. 2(b), of the number $\widehat{N}$ of points taken in the FFT for estimating g and $C_{\rm sca}$ for a sphere of diameter $D = 10\lambda$ and mesh size $d = \lambda/10$. For a given $\widehat{N}$, the sampling step Δk is equal to $2\pi/(d\widehat{N})$ so that the total number of points taken in the integration, N_o, is roughly equal to $\pi\left(d\widehat{N}/\lambda\right)^2$. Unsurprisingly, we observe that the errors on g and $C_{\rm sca}$ diminish with $\widehat{N}$. The improvement is particularly visible with the 3D FFT approach and comes from a better approximation of $k_z = \pm\sqrt{k_0^2 - k_x^2 - k_y^2}$ by $j_z \Delta k$ with j_z relative integer. The computation time of the classical approach increases linearly with N_o and is proportional to $\frac{N_x^3}{2}\pi\left(d\widehat{N}/\lambda\right)^2$ where $\frac{N_x^3}{2}$ is approximatively the number of dipoles that are needed to discretize the sphere. The computation time of the 2D FFT approach is proportional to $2N_x\widehat{N}^2\log(\widehat{N})$ (the multiplication by N_x is due to the integration along the z axis) while that of the 3D FFT approach is directly proportional to $3\widehat{N}^3\log(\widehat{N})$. Despite, these different behaviors, we observe that the computation-time of the FFT approaches, and especially that of the 2D FFT, is always much smaller than that of the classical approach by several orders of magnitude.

We now fix the number of points of the FFT to $\widehat{N} = 256$, the mesh size of the sphere to $d = \lambda/10$ (yielding $N_o \approx 8200$) and study the computation time Fig. 3(a) and accuracy Fig. 3(b) and (c) of the asymmetry parameter g and scattering cross-section $C_{\rm sca}$ of spheres of increasing diameter for the three different techniques. It is observed in Fig. 3 that, for a diameter range of the particles from 0 to 20λ, the 2D Fourier Method is always the most appropriate technique for estimating the scattering pattern with the less computation time. Indeed, the 3D approach has always a computational time larger that the 2D Fourier method approach due to the fact that N_x is always smaller than $\widehat{N}$ and moreover the relative error of the 3D FFT approach is significantly higher than that of the 2D technique due to the error made on k_z which is approximated by the nearest $j_z \Delta k$. As said previously, we note that the dashed line and the dotted line are confounded in Fig. 3(b) and (c) as the two approaches compute exactly the same integral.

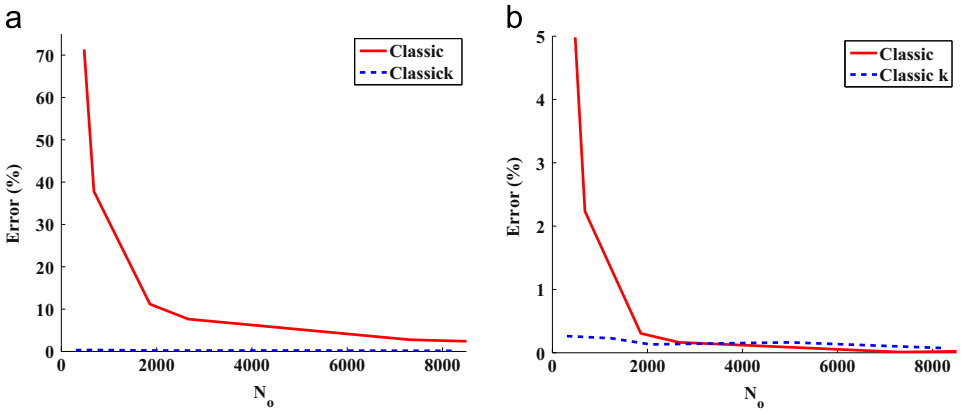

Fig. 1. Comparison of the integration performed in spherical coordinates (Classic) and Cartesian coordinates (Classic k) for estimating the scattering cross-section and the asymmetry parameter of a sphere of diameter 5λ of refractive index 1.1. (a) Relative error with respect to Mie result on the scattering cross section versus the number of points taken for calculating the integral. (b) same as (a) for the asymmetry parameter.

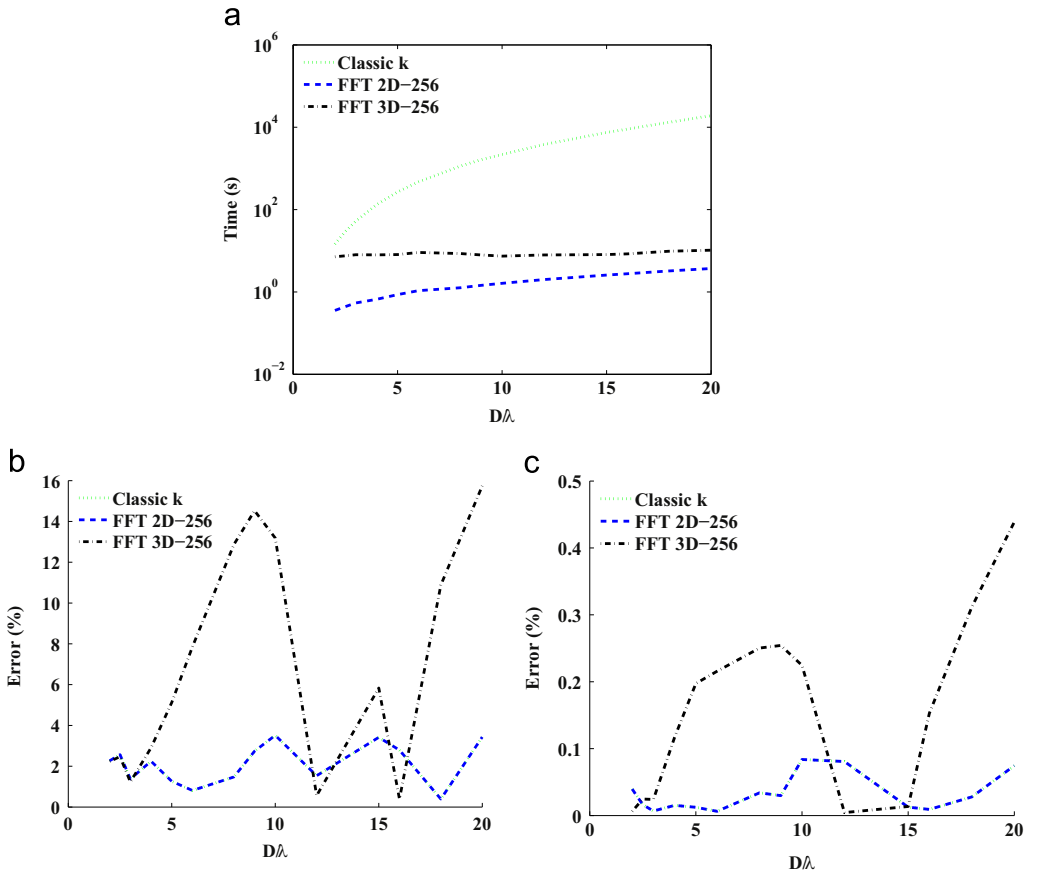

Fig. 2. Calculation of the scattering cross-section and asymmetry parameter of spheres with a diameter $D = 10\lambda$ versus $\hat{N}$ with three different methods (2D Fourier Transform (dashed line), 3D Fourier Transform (dot dashed line), classical integration in Cartesian coordinates (dotted line)). (a) Computation time required for the calculation as a function of $\hat{N}$. (b) Relative error in percent on the scattering cross-section. (c) Relative error in percent on the asymmetry parameter.

It is worth noting that, if the problem requires an estimation of the scattered field along only a few observation directions, it still may be advantageous to use the Fourier approach rather than the classical estimation. Indeed, if the sphere diameter is bigger than 20λ, the computation time of the estimation of 100×100 scattered-fields with the 2D Fourier Transform approach is comparable to that of 10 scattered fields with the classical approach. Notice that the 2D Fourier approach can be extended readily to more complex configurations where the scattering object is deposited on an interface or is buried in a multilayer. In this case, we observed exactly the same time gain as that presented in Fig. 3(a).

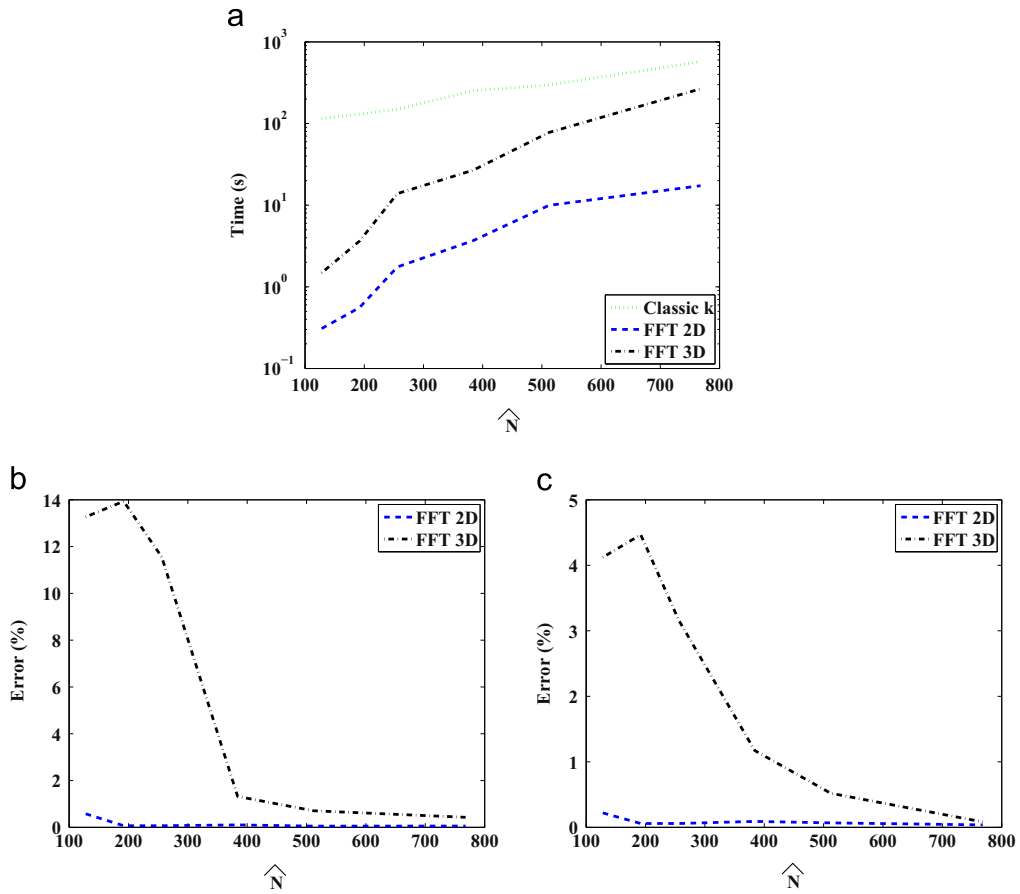

Fig. 3. Calculation of the scattering cross-section and asymmetry parameter of spheres with increasing diameter with three different methods (2D Fourier Transform (dashed line), 3D Fourier Transform (dot dashed line), classical integration in Cartesian coordinates (dotted line)). (a) Computation time required for the calculation as a function of the sphere diameter. (b) Relative error in percent on the scattering cross-section. (c) Relative error in percent on the asymmetry parameter.

4. Conclusion

In conclusion, we have dramatically accelerated the computation of scattered far-field in DDA by using Fast Fourier Transforms. This implementation should be most useful in configurations where the calculation of the scattered field is an important part of the total computation time, *i.e.* when the scattering object is large and weakly contrasted and when many observation angles are required (as in microscopy or flow cytometry experiments on biological objects).

Acknowledgments

This work has been financed by the ANR SURMITO.

References

[1] Kahnert FM. J Quant Spectrosc Radiat Transf 2003;79–80:775.
[2] Purcell EM, Pennypacker CR. Astrophys J 1973;186:705.
[3] Draine BT, Flatau PJ. J Opt Soc Am A 1994;11:1491.
[4] Yurkin MA, Hoekstra AG. J Quant Spectrosc Radiat Transf 2007;106:558.
[5] Flatau PJ, Stephens GL, Draine BT. J Opt Soc Am A 1990;7:593.
[6] Da Cunha RD, Hopkins T. Appl Numer Math 1995;19:33.
[7] Flatau PJ. Opt Lett 1997;22:1205.
[8] Chaumet PC, Rahmani A. Opt Lett 2009;34:917.
[9] Yurkin MA, Maltsev VP, Hoekstra AG. J Quant Spectrosc Radiat Transf 2007;106:546.
[10] Yurkin MA, Hoekstra AG. J Quant Spectrosc Radiat Transf 2011;112:2234.
[11] Flatau PJ, Draine BT. Opt Express 2012;20:1247.
[12] Zhang T, Godavarthi C, Chaumet PC, Maire G, nnini HG, Talneau A, et al. Opt Lett 2015;40:573.
[13] Zhang T, Ruan Y, Maire G, Sentenac D, Talneau A, Belkebir K, et al. Phys Rev Lett 2013;111:243904.
[14] Wang A, Dimiduk TG, Fung J, Razavi S, Kretzschmar I, Chaudhary K, et al. J Quant Spectrosc Radiat Transf 2014;146:499.
[15] Orlova DY, Yurkin MA, Hoekstra AG, Maltsev VP. J Biomed Opt 2008;13:054057.
[16] Draine BT. Astrophys J 1988;333:848.
[17] Chaumet PC, Sentenac A, Rahmani A. Phys Rev E 2004;70:036606.
[18] Smunev DA, Chaumet PC, Yurkin MA. J Quant Spectrosc Radiat Transf 2015;156:67.
[19] Hoekstra AG, Frijlink M, Waters LBFM, Sloot PMA. J Opt Soc Am A 2001;18:1944.